Efficient MPS methods for extracting spectral information on rings and cylinders

Maarten Van Damme,[1] Robijn Vanhove,[1] Jutho Haegeman,[1] Frank Verstraete,[1] and Laurens Vanderstraeten[1]

[1]*Department of Physics and Astronomy, University of Ghent, Krijgslaan 281, 9000 Gent, Belgium*

Based on the MPS formalism, we introduce an ansatz for capturing excited states in finite systems with open boundary conditions, providing a very efficient method for computing, e.g., the spectral gap of quantum spin chains. This method can be straightforwardly implemented on top of an existing DMRG or MPS ground-state code. Although this approach is built on open-boundary MPS, we also apply it to systems with periodic boundary conditions. Despite the explicit breaking of translation symmetry by the MPS representation, we show that momentum emerges as a good quantum number, and can be exploited for labeling excitations on top of MPS ground states. We apply our method to the critical Ising chain on a ring and the classical Potts model on a cylinder. Finally, we apply the same idea to compute excitation spectra for 2-D quantum systems on infinite cylinders. Again, despite the explicit breaking of translation symmetry in the periodic direction, we recover momentum as a good quantum number for labeling excitations. We apply this method to the 2-D transverse-field Ising model and the half-filled Hubbard model; for the latter, we obtain accurate results for, e.g., the hole dispersion for cylinder circumferences up to eight sites.

I. INTRODUCTION

Matrix product states (MPS) [1, 2], or the density-matrix renormalization group (DMRG) [3, 4], provide an efficient formalism for simulating one-dimensional (1-D) and quasi 1-D quantum lattice systems with very high precision. Although MPS are introduced most elegantly on a periodic system [5–7], MPS and DMRG algorithms are traditionally formulated on finite systems with open boundary conditions, because this setting allows for an efficient calculation of expectation values and the fixing of the gauge degrees of freedom in canonical forms. The disadvantage of open boundaries is that the translation symmetry of the model is explicitly broken, but the formulation of MPS directly in the thermodynamic limit [8–12] has made it possible to restore translational symmetries without sacrificing the efficiency or canonical forms of MPS. In this setting, translation symmetry of the MPS ground state has been used as a basis for formulating the MPS version [13] of the Feynman-Bijl ansatz [14] or the single-mode approximation [15–18], which describes excited-state wavefunctions with definite momentum quantum number with high precision for generic 1-D lattice models [19–21].

Yet, systems with periodic boundary conditions are important in, at least, two contexts. In both cases, periodic boundary conditions are used because the finite size effects are much smaller for systems with periodic as opposed to open boundary conditions. First, in the study of 1-D critical models the low-energy spectrum of a finite periodic system provides a very clear fingerprint of the conformal field theory (CFT) that captures the infrared properties of the model [22]. Therefore, computing the spectrum on a periodic system is paramount for identifying the effective CFT for a given critical model. Second, the finite size effects imply that the most efficient way of studying two-dimensional (2-D) quantum systems with MPS consists of imposing periodic boundary conditions in one direction, i.e. studying the model on a cylindrical geometry around which the MPS snakes or spirals.

In the case of 1-D periodic systems, there have been a number of proposals for alleviating the computational cost of periodic MPS [23–27] and DMRG [28, 29] simulations. In addition, a variational ansatz for capturing elementary excitations on top of a periodic MPS was proposed [30] and refined [27, 31], which captures many low-lying energy levels that reflect the CFT finite-size spectrum of critical spin chains[27]. Here, it is crucial that translation invariance is explicitly conserved in the ground state – by choosing a uniform MPS ansatz – such that the momentum is a good quantum number for labeling the excited states.

When systems with a cylindrical geometry are studied using a real space MPS ansatz [32], translation symmetry around the cylinder is explicitly broken by the MPS structure. While one can hope that the symmetry is restored in the ground state for sufficiently large bond dimension, transversal momentum cannot explicitly be used as a good quantum number in the MPS ansatz to target excitations. In the case of fermionic systems, one can switch to the momentum basis in the periodic direction such that translation symmetry can be preserved explicitly [33, 34]. In the case of spin systems, the transformation to the transversal momentum basis cannot be implemented as a canonical transformation and has as such not been considered, as it would not exhibit a tensor product structure.

In this paper, we show that we can recover momentum as a reliable quantum number to label excitations even when the associated translation symmetry is explicitly broken by the MPS structure. In particular, we will use open-boundary MPS and consider its tangent space as a variational ansatz for excitations, analogously to the excitation ansatz that has proven successful for infinite systems. First, we set the stage by applying this ansatz to an actual finite 1-D spin system, namely to study the magnon excitations in the spin-1 Heisenberg model, and compare the results to traditional DMRG-based approaches for targeting excited states. Next, we apply the same formalism to 1-D systems with periodic

boundary conditions, i.e. living on a ring, where we find that momentum is recovered with good accuracy. This is useful in particular for studying critical systems, and we obtain very accurate CFT spectra for Ising and Potts models. Finally, we translate the same idea to capturing excitations in infinite cylinders. Again, despite the explicit breaking of translation symmetry around the cylinder, the transversal momentum can be recovered accurately and we discuss a strategy to target specific momentum sectors. We illustrate this approach for the 2-D transverse-field Ising model and the half-filled 2-D Hubbard model. All algorithms in this paper can be found in *MPSKit.jl* [35], an open-source software package written in the scientific programming language Julia.

II. QUASIPARTICLES ON A FINITE SYSTEM

There are a variety of techniques to variationally target excited states in traditional DMRG or MPS simulations. The easiest is when the excitation has a non-trivial quantum number, such that it could directly be obtained as the solution of a ground state problem in that symmetry sector [4]. If multiple states in the same sector are required, they can be simultaneously captured by an extended DMRG procedure [4, 36], but the bond dimension grows rapidly with the number of targeted states. In the MPS representation, one would instead sequentially find higher excited states by imposing orthogonality on previously found states [37]. Finally, in the case of critical systems, it was realized recently that just changing one tensor in the middle of the chain is often sufficient to capture the low-lying excitations [38]. In this section, we introduce a variational ansatz for directly capturing the excited states of finite quantum chains and show that we can outperform these standard approaches, both in efficiency and accuracy.

A. Method

Let us consider a finite one-dimensional spin chain of length N with open boundary conditions, described by a generic model Hamiltonian H, for which the ground state is described by an MPS

$$|\Psi(A_1 \ldots A_N)\rangle = \boxed{A_1} - \boxed{A_2} - \boxed{\cdots} - \boxed{A_N}. \quad (1)$$

This MPS representation has a residual gauge freedom. In particular, we can always choose the tensors left and right of a given site to be respectively left and right isometries, leading to the representation

$$|\Psi(A_1 \ldots A_N)\rangle = \boxed{A_1^l} - \boxed{A_2^l} - \boxed{\cdots} - \boxed{A_i^c} - \boxed{\cdots} - \boxed{A_N^r}. \quad (2)$$

with A_i^l and A_i^r the left and right isometric MPS tensors, and A_i^c the center-site tensor. The standard sweeping algorithm [1] can be used to find an optimal MPS approximation for the ground state.

Once we have found a good MPS approximation of the ground state, we can build excitations on top. Inspired by the success of the quasiparticle ansatz in the thermodynamic limit, we propose a very similar ansatz

$$|\Phi(B_1, \ldots, B_N)\rangle = \sum_i \boxed{A_1^l} - \boxed{\cdots} - \boxed{B_i} - \boxed{\cdots} - \boxed{A_N^r}. \quad (3)$$

In this ansatz, we take a sum of N terms, where in each term we change one tensor. Note that one can represent this state as a finite MPS with two times the bond dimension of the ground state, but there are only $O(N\chi^2)$ free variational parameters.

The quasiparticle ansatz exhibits a gauge freedom, as every tensor B_i can be modified as $B_i' = B_i + X_i A_i^r - A_i^l X_{i+1}$ and we would still describe the same state. We can follow the ideas from infinite MPS [12], and fix this gauge freedom by imposing that B_i lives in the null-space of $(A_i^l)^\dagger$. The tensor B_i is then parametrized as

$$\boxed{B_i} = \boxed{V_i} - \boxed{X_i} \quad (4)$$

where X_i contains the actual degrees of freedom and V_i spans the null space of $(A_i^l)^\dagger$, i.e. it contains the orthonormal columns to complement A_i^l to a full unitary matrix. As a consequence, the quasiparticle state is automatically orthogonal to the ground-state MPS. Our ansatz now becomes

$$|\Phi(X_1 \ldots X_N)\rangle = \sum_i |\Phi_i(X_i)\rangle,$$
$$|\Phi_i(X_i)\rangle = \boxed{A_1^l} - \boxed{\cdots} - \boxed{V_i} - \boxed{X_i} - \boxed{\cdots} - \boxed{A_N^r}. \quad (5)$$

The overlap of two distinct quasiparticle states simplifies to the simple euclidean inner product[1] of the tensors X_i

$$\langle \Phi(X_1 \ldots X_N) | \Phi(X_1' \ldots X_N') \rangle = \sum_i (\vec{X}_i)^\dagger X_i'$$
$$= (\vec{X}')^\dagger \vec{X} \quad (6)$$

This is important, as minimizing the energy within the manifold of quasiparticle excitations now becomes a simple eigenvalue problem

$$\sum_j (H_{\text{eff}})_{ij} \vec{X}_j = \omega \vec{X}_i, \quad (7)$$

with the effective hamiltonian matrix

$$(\vec{X}_i)^\dagger (H_{\text{eff}})_{ij} \vec{X}_j = \langle \Phi_i(X_i) | H | \Phi_j(X_j) \rangle. \quad (8)$$

The action of H_{eff} on a set of tensor X_i can be computed easily, and the eigenvalue problem can be solved by an iterative Krylov method, typically the Lanczos method.

---

[1] Here we denote $\vec{X}_i$ for the vectorized version of the tensor X, and $\vec{X}$ for the concatenation of the vectors $\vec{X}_i$ into a large vector.
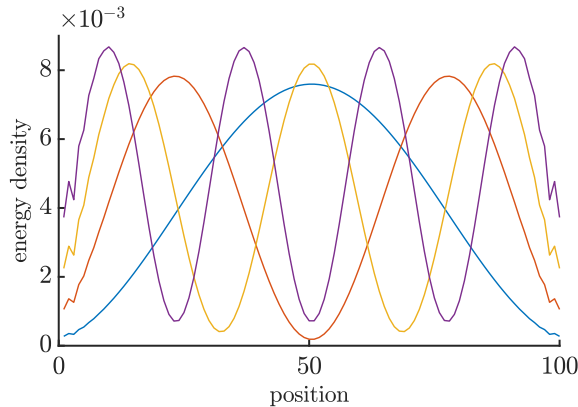
FIG. 1. The energy density of the four lowest-lying spin-1 magnon excitations on top of the ground state of the spin-1 Heisenberg chain with 100 sites. The ground state has bond dimension $D = 64$.

Energy QP	Energy DMRG	Variance QP	Variance DMRG
0.4165739	0.4165864	3.1e-6	7.05e-5
0.4165739	0.4165865	3.1e-6	7.09e-5
0.4165739	0.4165864	3.1e-6	7.05e-5
0.4344129	0.4344322	3.2e-6	0.00011
0.4344129	0.4344321	3.2e-6	0.000109
0.4344129	0.4344321	3.2e-6	0.000109
0.462799	0.4628202	3.3e-6	0.0001207
0.462799	0.4628204	3.3e-6	0.0001209
0.462799	0.4628205	3.3e-6	0.0001209
0.5001103	0.5001329	3.3e-6	0.000129

TABLE I. Comparison of the energies and energy variances obtained using the quasiparticle (QP) ansatz and using DMRG, for the lowest-lying excitations in the spin-1 chain with N sites (also see Fig. 1). For the DMRG excitations, the maximum number of sweeps was set at 100.

B. Magnon in the spin-1 chain

In infinite systems, the excitation ansatz leads to a picture of gapped excitations as dressed quasiparticles against a correlated background state [39]; in that setting the ansatz describes a traveling wave or Bloch wave with a definite momentum. On a finite system with open boundary conditions, however, we would expect to find a standing-wave configuration of this very same dressed particle.

As an illustration of this scenario, we simulate the excitation spectrum of the spin-1 Heisenberg chain on a finite system with open boundary conditions. In order to focus on the bulk excitations, we place spin-1/2s at the ends, thus eliminating the gapless edge modes[40]. In Fig. 1 we plot the energy density of the first five excited states, showing indeed the different standing-wave patterns of the magnon behaving as a particle-in-a-box [41].

We can compare this method for extracting excited states with the conventional MPS methods. As explained above, the standard method requires an entire sweeping optimization for every excited state, and one needs higher bond dimensions to faithfully capture the excitation. In that respect, the quasiparticle ansatz is numerically much cheaper as it only requires to solve a single eigenvalue problem for a given number of excited states. Moreover, the excitation ansatz reaches the same level of accuracy for the energy, as we show explicitly in Table I. One expects the excitation ansatz to fail for higher excitations, as soon as they start to involve multiple particles. It then makes sense to go to a hybrid setup where we switch to DMRG after the first few lowest eigenvectors. This will not be necessary however when doing simulations of a system close to criticality and for which the correlation length of the MPS is larger than the system size (i.e. the finite size scaling regime): in that case, the local tensors in the quasiparticle ansatz have a global effect, and seem to be able to represent multiparticle excitations [38].

III. CRITICAL SYSTEMS ON A RING

As highlighted above, MPS techniques are significantly less efficient for systems with periodic boundary conditions, in part due do the inferior scaling in bond dimension when using an MPS with periodic boundary conditions. Still, both ground states and excited states can be targeted with high precision using periodic MPS.

An alternative approach is to re-use the above technique for open boundary systems, but with a periodic hamiltonian or transfer matrix. Although it would require a quadratically larger bond dimension to represent a periodic MPS as an open-boundary MPS, we will show that we obtain quantitatively good results at reasonable bond dimensions. In particular, we can compute the expectation value of the translation operator, which for the MPS ground state [Eq. 1] is given by

$$\langle \Psi(A_1 \dots) | \, T \, | \Psi(A_1 \dots) \rangle = \quad , \quad (9)$$

and show that the momentum of the ground states, as well as the excited states[2], are correct up to very high precision.

In Ref. 27 it was shown that the excitation ansatz for periodic MPS is able to reproduce a surprising number of energy levels in the finite-size CFT spectrum of critical

----

[2] Eigenvalues occur with different degeneracies and the corresponding eigenvectors will be momentum superpositions. We then have to diagonalize the translation operator within this degenerate-energy subspace to extract the momentum labels. It is also possible to work the other way around, and impose a certain momentum. That is precisely what we do in the next section, for quantum systems on a cylinder.
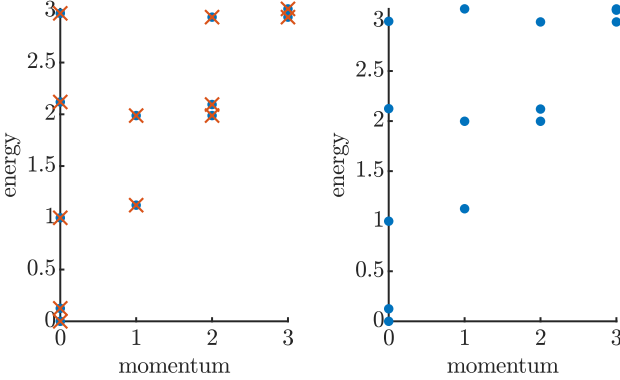
FIG. 2. The lowest-lying energy levels for the quantum Ising chain on a circle with circumferences $N = 20$ (left) and $N = 50$ (right). The blue dots are results from the MPS excitation ansatz with $D = 50$ and the red crosses are results from exact diagonalization. The energies were shifted and rescaled such that the ground state is at $e_0 = 0$ and the gap $\Delta_\epsilon = 1$. We see that the MPS with open boundary conditions restores translation invariance, and that degeneracies agree with exact results.

spin chains – even the multi-particle excitations are well captured by this ansatz. In order to make this possible, the bond dimension of the ground-state MPS needs to be large enough such that we are in the finite-size scaling regime [25]: through the virtual level of the MPS one can change the state over the whole system by modifying a single tensor locally. This same effect was observed in Ref. [38] for systems with open boundary conditions. Motivated by this effect, we now apply our open-boundary MPS excitation ansatz to critical models on a ring.

A. Quantum Ising chain

Let us first look at the simplest critical 1-D model, the critical Ising chain. As shown in Fig. 2, our results agree well with exact diagonalization. Despite the open boundary conditions, the MPS restores translation invariance and we retrieve momentum eigenstates. Because our method does not scale exponentially in system size, we can push the simulation to much higher system sizes. This is important for systems with a large local dimension, where one often cannot reach large enough sizes to perform finite-size scaling.

B. Classical 2-D Potts model

We can also deal with statistical-mechanical problems on an infinite cylinder, by finding the leading eigenvectors of the transfer matrix [42] in the periodic direction. The largest few eigenvalues contain information about the free energy and the dominant correlation functions
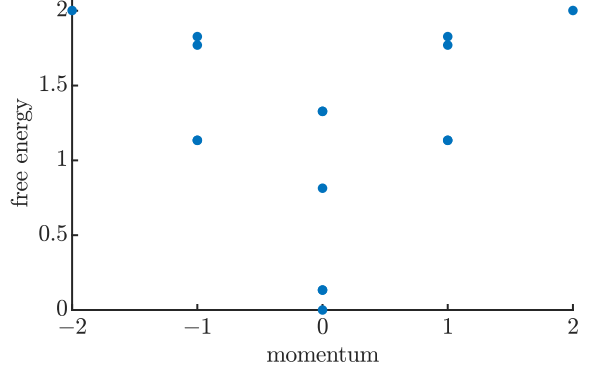

FIG. 3. The rescaled spectrum of the transfer matrix of the 3-state Potts model with system size $N = 28$, as obtained with the excitation ansatz with bond dimension $D = 150$. We take the negative logarithm of the transfer-matrix eigenvalues, $f = -\log \lambda$, such that f corresponds to a free energy. We have rescaled the values such that fixed-point free energy is set at $f = 0$ and the first excited state at $f = 2/15$.

in the system. It is possible to find the dominant eigenvector by modifying any of the well known ground-state algorithms to look for the largest magnitude eigenvector, and the above algorithm for finding the excited states of the transfer matrix are straightforwardly adapted.

Here we show the finite-size spectrum of the critical 3-state Potts model. In Fig. 3 we show the spectrum of the transfer matrix with circumference $N = 28$ – a system size that is not feasible with exact diagonalization – at bond dimension $D = 150$. The rescaling was done such that the ground state sits at free energy $f = 0$ and the first excited state at $f = 2/15$ (the smallest non-trivial scaling dimension for the Potts CFT); all other eigenvalues are approaching the CFT prediction. In Tab. II we compare the obtained energies with both the exact results on smaller systems and the CFT prediction for the infinite-size limit. An alternative rescaling could be performed, where the free energy at momentum 2 is rescaled such that it lies at free energy $f = 2$ (the first excited state of the identity tower), exploiting the momentum information explicitly. Such a rescaling is independent of the CFT [22], but looking at Tab. II at $N = 28$, it makes almost no difference compared to the rescaling that we have used.

IV. SYSTEMS ON A CYLINDER

We can generalize this approach to the setting of MPS approximations for cylindrical systems, a setup that is very often used for simulating 2-D systems. Here, the MPS is wrapped around the infinite cylinder in a snake-like fashion, so the translation symmetry in the transverse direction is explicitly broken by the MPS representation. However, just like for the one-dimensional rings above,

10	12	14	28	CFT
0.0	0.0	0.0	0.0	0.0
0.13333	0.13333	0.13333	0.13333	0.13333
0.13333	0.13333	0.13333	0.13333	0.13333
0.83376	0.82863	0.82499	0.8139	0.8
1.148	1.1428	1.1398	1.134	1.1333
1.148	1.1428	1.1398	1.134	1.1333
1.148	1.1428	1.1398	1.134	1.1333
1.148	1.1428	1.1398	1.134	1.1333
1.3213	1.3225	1.3235	1.3277	1.3333
1.3213	1.3225	1.3235	1.3277	1.3333
1.7462	1.75	1.7537	1.7704	1.8
1.7462	1.75	1.7537	1.7704	1.8
1.8995	1.8763	1.8618	1.8272	1.8
1.8995	1.8763	1.8618	1.8272	1.8
2.0532	2.0336	2.0224	2.0016	2.0
2.0532	2.0336	2.0224	2.0017	2.0

TABLE II. Comparison of the rescaled free energies of the 3-state Potts model at different system sizes with the CFT prediction. Results for system sizes $N = (10, 12, 14)$ were obtained with exact diagonalization, while results for system size $N = 28$ where obtained with our MPS-based excitation ansatz with bond dimension $D = 150$.

we can hope that this translation symmetry is restored for large enough bond dimensions and that we can exploit this to create quasiparticle excitations with fixed transverse momentum. In the case of infinite cylinders, translation symmetry along the cylinder can be imposed straightforwardly, so in this way we can have access to the momentum quantum numbers in both directions.

A. Method

The ground state of an infinite cylinder with a circumference of N sites can be represented by an infinite MPS with an N-site unit cell[3]

$$|\Psi(\{A_i\})\rangle = \cdots \boxed{A_1} \cdots \boxed{A_N} \boxed{A_1} \cdots \boxed{A_N} \cdots . \quad (10)$$

This MPS can be found using variational ground-state searches [12, 43] or the infinite DMRG algorithm [10]. We normalize the state such that the leading eigenvalue of the N-site transfer matrix is one,

$$\lambda_{\max}\left(\begin{array}{c} \boxed{A_1} \cdots \boxed{A_N} \\ \boxed{A_1} \cdots \boxed{A_N} \end{array} \right) = 1. \quad (11)$$

_____

[3] The analysis is easily generalized to larger unit cells.

There are two translation operators acting on this state. The first one (T_x) corresponds to translation along the cylinder, and shifts the full unit cell

$$T_x |\Psi(\{A_i\})\rangle = \boxed{A_1} \cdots \boxed{A_N} \boxed{A_1} \cdots \boxed{A_N} . \quad (12)$$

The second one (T_y) corresponds to translation around the cylinder and is a transformation within the unit cell,

$$T_y |\Psi(\{A_i\})\rangle = \boxed{A_1} \cdots \boxed{A_N} \boxed{A_1} \cdots \boxed{A_N} . \quad (13)$$

The MPS is invariant under T_x by construction, but translation invariance under T_y is less trivial. The expectation value of this operator

$$\langle\Psi(\{A_i\})| T_y |\Psi(\{A_i\})\rangle , \quad (14)$$

is a quantity that scales exponentially with the number of unit cells, so the characteristic quantity is the leading eigenvalue of the mixed N-site transfer matrix,

$$\mu = \lambda_{\max}\left(\begin{array}{c} \boxed{A_1} \boxed{A_2} \cdots \boxed{A_N} \\ \boxed{A_1} \boxed{A_2} \cdots \boxed{A_N} \end{array} \right), \quad (15)$$

so that, formally, $\langle\Psi(\{A_i\})| T_y |\Psi(\{A_i\})\rangle \sim \mu^{N_x}$ with N_x the diverging number of unit cells. For future reference, we can associate left and right fixed points to this mixed transfer matrix as

$$l \begin{array}{c} \boxed{A_1} \boxed{A_2} \cdots \boxed{A_N} \\ \boxed{A_1} \boxed{A_2} \cdots \boxed{A_N} \end{array} = \mu \, l \quad (16)$$

$$\begin{array}{c} \boxed{A_1} \boxed{A_2} \cdots \boxed{A_N} \\ \boxed{A_1} \boxed{A_2} \cdots \boxed{A_N} \end{array} r = \mu \, r . \quad (17)$$

Now the MPS has well-defined transverse momentum if the eigenvalue μ lies on the unit circle with the angle a multiple of $2\pi/N$.

We can make an excitation on top of this MPS with the ansatz

$$|\Phi_{p_x}(B)\rangle = \sum_n e^{ip_x n} T_x^n$$

$$\boxed{A_1} \Box \boxed{A_N} \boxed{\quad B \quad} \boxed{A_1} \Box \boxed{A_N} \quad (18)$$

with

$$\boxed{\quad B \quad} = \boxed{B_1} \cdots \boxed{A_N} + \ldots$$

$$\cdots + \boxed{A_1} \cdots \boxed{B_N} . \quad (19)$$

This is the multi-site version [20] of the excitation ansatz [13] for infinite MPS. Similar to Eq. 4, we can fix the redundant gauge degrees of freedom in the B tensors such

that the overlap between two of these excited states reduces to the simple euclidean inner product with a δ-function normalization for the momentum,

$$\langle\Phi_{p_x'}(B')|\Phi_{p_x}(B)\rangle = 2\pi\delta(p_x-p_x')\sum_{i=1}^N(\vec{B_i'})^\dagger\vec{B_i}. \quad (20)$$

Consequently, an ordinary eigenvalue problem

$$H_{p_x,\text{eff}}\vec{B} = \omega\vec{B}, \quad (21)$$

with

$$\langle\Phi_{p_x'}(B')|\,H\,|\Phi_{p_x}(B)\rangle$$
$$= 2\pi\delta(p_x-p_x')(\vec{B})^\dagger H_{p_x,\text{eff}}\vec{B}, \quad (22)$$

finds the optimal B tensors for representing the lowest-energy excitation in the system.

This ansatz clearly is an eigenstate of the T_x operator,

$$T_x\,|\Phi_{p_x}(B)\rangle = \mathrm{e}^{ip_x}\,|\Phi_{p_x}(B)\rangle, \quad (23)$$

but the momentum around the cylinder is not straightforward. Indeed, we can compute the normalized expectation value for the T_y operator by dividing by the ground-state expectation value

$$\frac{1}{2\pi\delta(p_x-p_x')}\frac{\langle\Phi_{p_x'}(B)|\,T_y\,|\Phi_{p_x}(B)\rangle}{\langle\Psi(A)|\,T_y\,|\Psi(A)\rangle}$$

$$+\dots, \quad (24)$$

The infinite sums in this expression converge so that this expression yields a finite number; we can hence compute the transverse momentum of the excited states that we find variationally. We can, however, directly target excitations that are approximate eigenvectors of the T_y operators. Indeed, if we define the effective T_y operator as

$$\frac{\langle\Phi_{p_x}(B')|\,T_y\,|\Phi_{p_x}(B)\rangle}{\langle\Psi(A)|\,T_y\,|\Psi(A)\rangle} = 2\pi\delta(p_x-p_x')(\vec{B'})^\dagger T_{\text{eff}}\vec{B}, \quad (25)$$

we solve the eigenvalue problem

$$\left(H_{p_x,\text{eff}} - \alpha\mathrm{e}^{-ip_y}T_{\text{eff}}\right)B_{p_x,p_y} = \lambda B_{p_x,p_y} \quad (26)$$

for the eigenvalue $\lambda = \omega - \alpha$ with the most negative real part.[4] When α is sufficiently large and translation

_____

[4] It would be more elegant to consider the operator

$$H_{p_x,\text{eff}} - \alpha\mathrm{e}^{-ip_y}T_{\text{eff}} - \alpha\mathrm{e}^{ip_y}T_{\text{eff}}^\dagger, \quad (27)$$

such that the eigenvalue problem remains hermitian. In practice, however, we find that adding the hermitian conjugate is not needed for the stability of the eigenvalue problem and only increases the computational cost.
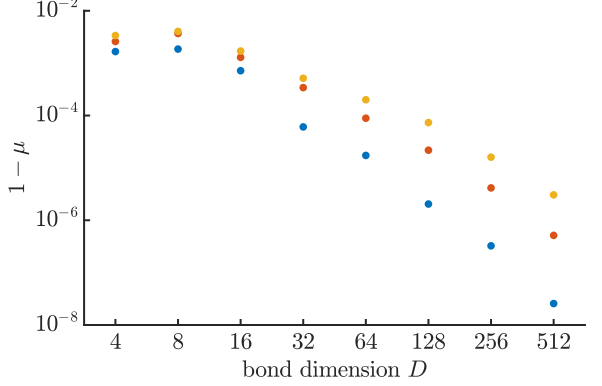
FIG. 4. The momentum per rung of the MPS ground state [Eq. 15] for the square-lattice Ising model on an $N = 12$ cylinder as a function of bond dimension for three values of the field, $\lambda = 2.5$ (blue), $\lambda = 2.9$ (red) and $\lambda = 3.04438$ (orange).

symmetry is sufficiently well captured by the MPS, this eigenvalue should indeed be real and correspond to an eigenstate with transversal momentum p_y and energy eigenvalue ω.

B. Benchmarks

We first illustrate this approach on the two-dimensional transverse-field Ising model, defined by the Hamiltonian

$$H_{\text{Ising}} = \sum_{\langle ij\rangle}S_i^z S_j^z + \lambda\sum_i S_i^x. \quad (28)$$

We choose to run simulations at two values in the symmetry-broken phase, $\lambda = 2.5$ and $\lambda = 2.9$, and at the quantum critical point $\lambda = 3.04438$ (taken from Ref. 44).

Let us first consider the momentum of the MPS ground state. We have optimized MPS ground states on infinite cylinders with circumference $N = 12$ at different bond dimensions, showing that the expectation value of T_y per rung [Eq. 15] nicely converges to one. The convergence is slower as one approaches the critical point, which points to the fact that a larger bond dimension is needed near criticality.

Next we study the excitations, where we can take different cuts of the two-dimensional Brillouin zone by imposing the transverse momentum as in Eq. (26), see Fig. 5. The $p_y = 0$ cut shows the dispersion becoming gapless at the critical point, whereas the $p_y = \pi$ is gapped. We push the bond dimension to get a good estimate for the gapless point, showing that the finite circumference induces a non-zero gap even for the critical value of the field; only in the infinite 2-D plane the model becomes truly gapless. As we show in the bottom panel of Fig. 5, the finite-size gap decreases for increasing cylinder width.
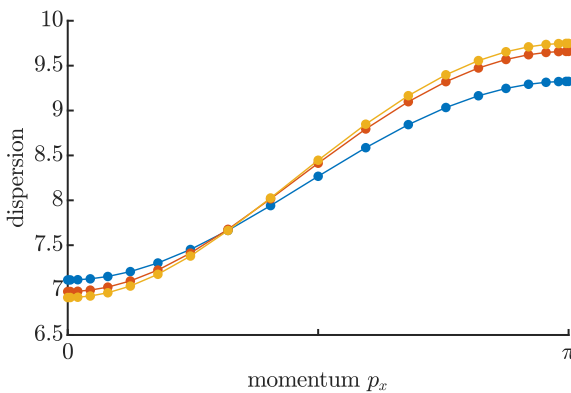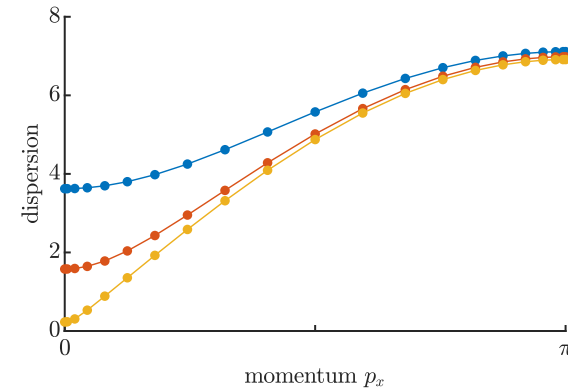
FIG. 5. The dispersion relation of the square-lattice Ising model on a cylinder of circumference $N = 12$ for three values of the field, $\lambda = 2.5$ (blue), $\lambda = 2.9$ (red) and $\lambda = 3.04438$ (orange). The top panel show the BZ cut at transverse momentum $p_y = 0$, nicely capturing the spectrum becoming gapless at the critical point. The bottom panel is for $p_y = \pi$, where the dispersion changes very little as the field is tuned. Here, all simulations were done with an MPS bond dimension $D = 256$.
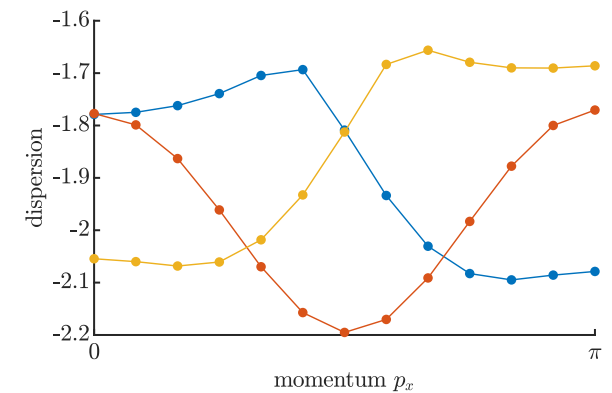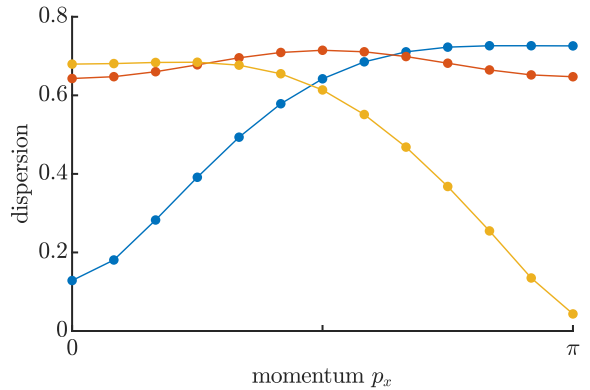

FIG. 7. The dispersion relation of the Hubbard model with $t = 1$ and $U = 12$ on a cylinder of circumference $N = 4$, in three cuts of the Brillouin zone $p_y = 0$ (blue), $p_y = \pi/2$ (red) and $p_y = \pi$ (orange). The top panel shows the dispersion of the magnon excitation (charge-neutral spin-1 excitation) in three momentum cuts, and the bottom panel shows the hole dispersion (charged spin-1/2 excitation). Here, the total bond dimension is around $D = 3500$, where the largest SU(2)⊗U(1) symmetry block is $D_{\max} = 154$.
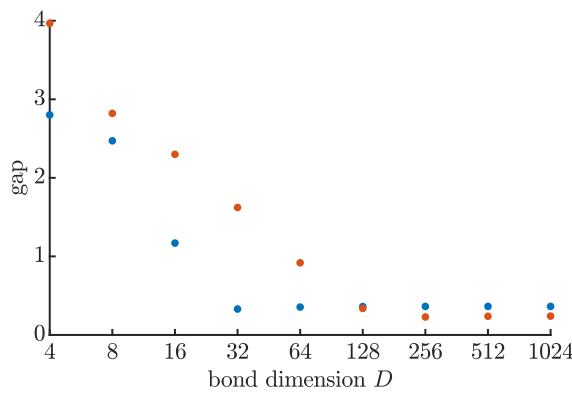

FIG. 6. The bottom panel shows the gap at $\lambda = 3.04438$ for cylinders $N = 8$ (blue) and $N = 12$ (red). We can converge the value of the gap with increasing bond dimension in both cases, although the larger cylinder needs higher bond dimension. The non-zero gap is due to the finite circumference of the cylinder, and clearly goes down as N increases.
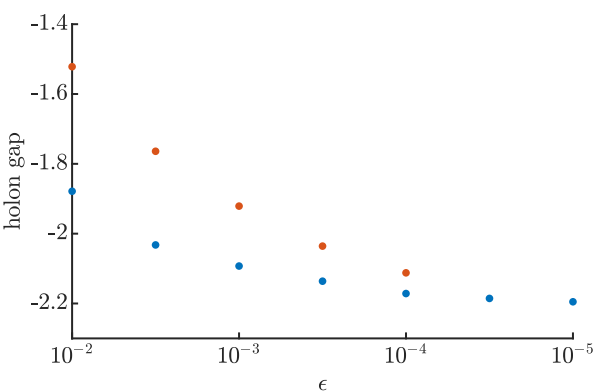

FIG. 8. The minimum of the dispersion relation at the S point for the $N = 4$ (blue) and the $N = 8$ (red) cylinder as a function of truncation threshold of the MPS.

Now we apply our method to the two-dimensional Hubbard model on the square lattice at half filling, with Hamiltonian

$$H_{\text{Hubbard}} = -\sum_{\sigma=\{\uparrow,\downarrow\}} \sum_{\langle ij \rangle} \left(c_{\sigma,i}^\dagger c_{\sigma,j} + c_{\sigma,j}^\dagger c_{\sigma,i} \right)$$
$$+ U \sum_i \left(c_{\uparrow,i}^\dagger c_{\uparrow,i} \right) \left(c_{\downarrow,i}^\dagger c_{\downarrow,i} \right), \quad (29)$$

where $c_{\sigma,i}$ and $c_{\sigma,i}^\dagger$ are fermionic creation and annihilation operators with spin σ at site i. In our MPS representation for the ground state on the cylinder, we fix the filling by implementing the U(1) symmetry for the electron charge, use SU(2) spin-rotation symmetry (which is left unbroken on a cylinder with finite circumference) and implement a graded $\mathbb{Z}_2$ symmetry [45] for encorporating fermionic statistics. We work at $U = 12$, deep in the Mott-insulating phase.

We optimize the ground state on infinite cylinders of circumference $N = 4$ and $N = 8$ using the vumps algorithm [43], and look at the excitation spectrum on top of the ground state. Using the U(1) and SU(2) symmetries in the MPS representation, we can fix the charge and spin quantum numbers (q_c, q_s) in the excited state ansatz.

First, we study the magnon excitations with quantum numbers $(0, 1)$ in the top panel of Fig. 7. We observe a strong minimum in the X-point at (π, π), in agreement with the fact that the model effectively behaves as a Heisenberg antiferromagnet in the charge-neutral sector. We also see a minimum at $(0, 0)$, corresponding to a two-magnon state. We observe that the magnon gap at (π, π) converges quickly with bond dimension, which points to the fact that the magnon is a well-defined quasiparticle for which our ansatz is ideally suited. Correspondingly, we observe that the energy of the two-magnon state at $(0, 0)$ converges a lot slower (not shown).

Next, we consider the charged excitations with quantum numbers $(-1, \frac{1}{2})$. The hole dispersion can be directly observed in angle-resolved photoemission spectroscopy, and has gained a lot of (renewed) theoretical attention due to recent cold-atom experiments [46, 47]. In particular, the nature of the magnetic polaron as a bound state of chargon and spinon [48–50] has been investigated in some detail. In the bottom panel of Fig. 7 we have plotted three momentum cuts for the $N = 4$ cyinder, and we observe a minimum in the S point at $(\pi/2, \pi/2)$. This feature is in agreement with a recent numerical study of the t-J model [50]. The $p_y = 0$ and $p_y = \pi$ cuts also show pronounced minima, and a level crossing at higher energies.

In Fig. 8 we plot this minimum of the hole dispersion, i.e. the charge gap, as a function of Schmidt-value threshold[5] in the MPS ground state for the $N = 4$ and

the $N = 8$ cylinders. We observe that convergence is rather slow, which points to the composite nature of the excitation: The quasiparticle ansatz needs a large bond dimension for describing the extended bound-state complex. As Fig. 8 shows, the charge gap is not completely converged for the $N = 8$ cylinder with our highest bond dimension ($D \approx 7000$), but presumably a larger-scale simulation could find a fully converged value also for the eight-site cylinder.

V. CONCLUSIONS

In this paper we have applied open-boundary MPS algorithms to systems with periodic boundary conditions. In particular, although translation symmetry is broken by the MPS representation, we have shown that momentum emerges as a good quantum number. This can be exploited for labeling excitations on top of MPS ground states.

We have also introduced an ansatz for capturing excited states in finite systems with open boundary conditions, which is a very efficient method for computing e.g. the spectral gap, and which can be straightforwardly implemented on top of an existing DMRG or MPS ground-state code. We expect that this approach can be of great use to the DMRG/MPS community.

Our method was shown to work very well for obtaining CFT finite-size spectra of critical models. We expect this will prove useful for characterizing the effective CFT for 1-D quantum and 2-D classical models, as well as to compute entanglement spectra of projected entangled-pair states in order to characterize the (chiral) edge field theory [51].

Applying the framework to 2-D cylinders has shown that we can obtain excitation spectra of challenging models such as spin liquids or (doped) Hubbard models. Indeed, whereas simulating time evolution is often prohibitively expensive for these models and excitation spectra are, therefore, rather infeasible to compute, the excitation ansatz can be applied with a cost that is similar to a ground-state simulation. In that respect, it would be extremely interesting to look at fractionalized excitations such as spinons or holons: In principle, the excitation ansatz can be straightforwardly generalized to also capture these topological excitations [20, 52]. Another interesting question is how this MPS excitation ansatz on the cylinder compares to the excitation ansatz for projected entangled-pair states [53–55], which is formulated directly on the infinite plane.

_____

[5] The Schmidt-value threshold is the approximate value of the

smallest Schmidt value in all symmetry sectors of the MPS; it is the analog of the truncation threshold in (i)DMRG simulations, which does not have a clear meaning in variational optimization schemes without truncation steps.

VI. ACKNOWLEDGEMENTS

[1] U. Schollwöck, The density-matrix renormalization group in the age of matrix product states, Annals of Physics **326**, 96 (2011).

[2] J. I. Cirac, D. Perez-Garcia, N. Schuch, and F. Verstraete, Matrix product states and projected entangled pair states: Concepts, symmetries, and theorems, arXiv:2011.12127 (2020).

[3] S. R. White, Density matrix formulation for quantum renormalization groups, Phys. Rev. Lett. **69**, 2863 (1992).

[4] S. R. White, Density-matrix algorithms for quantum renormalization groups, Phys. Rev. B **48**, 10345 (1993).

[5] S. Rommer and S. Östlund, Class of ansatz wave functions for one-dimensional spin systems and their relation to the density matrix renormalization group, Phys. Rev. B **55**, 2164 (1997).

[6] F. Verstraete, D. Porras, and J. I. Cirac, Density matrix renormalization group and periodic boundary conditions: A quantum information perspective, Phys. Rev. Lett. **93**, 227205 (2004).

[7] D. Perez-Garcia, F. Verstraete, M. M. Wolf, and J. I. Cirac, Matrix product state representations, arXiv:quant-ph/0608197 (2006).

[8] S. Östlund and S. Rommer, Thermodynamic limit of density matrix renormalization, Phys. Rev. Lett. **75**, 3537 (1995).

[9] G. Vidal, Classical simulation of infinite-size quantum lattice systems in one spatial dimension, Phys. Rev. Lett. **98**, 070201 (2007).

[10] I. P. McCulloch, Infinite size density matrix renormalization group, revisited, arXiv:0804.2509 (2008).

[11] J. Haegeman, J. I. Cirac, T. J. Osborne, I. Pižorn, H. Verschelde, and F. Verstraete, Time-dependent variational principle for quantum lattices, Phys. Rev. Lett. **107**, 070601 (2011).

[12] L. Vanderstraeten, J. Haegeman, and F. Verstraete, Tangent-space methods for uniform matrix product states, SciPost Phys. Lect. Notes , 7 (2019).

[13] J. Haegeman, B. Pirvu, D. J. Weir, J. I. Cirac, T. J. Osborne, H. Verschelde, and F. Verstraete, Variational matrix product ansatz for dispersion relations, Phys. Rev. B **85**, 100408 (2012).

[14] R. P. Feynman, Atomic theory of the λ transition in helium, Phys. Rev. **91**, 1291 (1953).

[15] S. M. Girvin, A. H. MacDonald, and P. M. Platzman, Collective-excitation gap in the fractional quantum hall effect, Phys. Rev. Lett. **54**, 581 (1985).

[16] D. P. Arovas, A. Auerbach, and F. D. M. Haldane, Extended heisenberg models of antiferromagnetism: Analogies to the fractional quantum hall effect, Phys. Rev. Lett. **60**, 531 (1988).

[17] M. Takahashi, Excitation spectra of s=1 antiferromagnetic chains, Phys. Rev. B **50**, 3045 (1994).

[18] E. S. Sørensen and I. Affleck, Equal-time correlations in haldane-gap antiferromagnets, Phys. Rev. B **49**, 15771 (1994).

[19] A. K. Bera, B. Lake, F. H. L. Essler, L. Vanderstraeten, C. Hubig, U. Schollwöck, A. T. M. N. Islam, A. Schneidewind, and D. L. Quintero-Castro, Spinon confinement in a quasi-one-dimensional anisotropic heisenberg magnet, Phys. Rev. B **96**, 054423 (2017).

[20] V. Zauner-Stauber, L. Vanderstraeten, J. Haegeman, I. P. McCulloch, and F. Verstraete, Topological nature of spinons and holons: Elementary excitations from matrix product states with conserved symmetries, Phys. Rev. B **97**, 235155 (2018).

[21] L. Vanderstraeten, M. Van Damme, H. P. Büchler, and F. Verstraete, Quasiparticles in quantum spin chains with long-range interactions, Phys. Rev. Lett. **121**, 090603 (2018).

[22] P. Francesco, P. Mathieu, and D. Sénéchal, *Conformal field theory* (Springer Science & Business Media, 2012).

[23] D. Porras, F. Verstraete, and J. I. Cirac, Renormalization algorithm for the calculation of spectra of interacting quantum systems, Phys. Rev. B **73**, 014410 (2006).

[24] B. Pirvu, F. Verstraete, and G. Vidal, Exploiting translational invariance in matrix product state simulations of spin chains with periodic boundary conditions, Phys. Rev. B **83**, 125104 (2011).

[25] B. Pirvu, G. Vidal, F. Verstraete, and L. Tagliacozzo, Matrix product states for critical spin chains: Finite-size versus finite-entanglement scaling, Phys. Rev. B **86**, 075117 (2012).

[26] D. Draxler, J. Haegeman, F. Verstraete, and M. Rizzi, Continuous matrix product states with periodic boundary conditions and an application to atomtronics, Phys. Rev. B **95**, 045145 (2017).

[27] Y. Zou, A. Milsted, and G. Vidal, Conformal data and renormalization group flow in critical quantum spin chains using periodic uniform matrix product states, Phys. Rev. Lett. **121**, 230402 (2018).

[28] P. Pippan, S. R. White, and H. G. Evertz, Efficient matrix-product state method for periodic boundary conditions, Phys. Rev. B **81**, 081103 (2010).

[29] D. Rossini, V. Giovannetti, and R. Fazio, Stiffness in 1d matrix product states with periodic boundary conditions, Journal of Statistical Mechanics: Theory and Experiment **2011**, P05021 (2011).

[30] B. Pirvu, J. Haegeman, and F. Verstraete, Matrix product state based algorithm for determining dispersion relations of quantum spin chains with periodic boundary conditions, Phys. Rev. B **85**, 035130 (2012).

[31] W.-L. Tu, H.-K. Wu, N. Schuch, N. Kawashima, and J.-Y. Chen, Generating function for tensor network diagrammatic summation, arXiv:2101.03935 (2021).

[32] E. M. Stoudenmire and S. R. White, Studying two-dimensional systems with the density matrix renormalization group, Annual Review of Condensed Matter Physics **3**, 111 (2012).

[33] J. Motruk, M. P. Zaletel, R. S. K. Mong, and F. Pollmann, Density matrix renormalization group on a cylin-

der in mixed real and momentum space, Phys. Rev. B **93**, 155139 (2016).

[34] G. Ehlers, S. R. White, and R. M. Noack, Hybrid-space density matrix renormalization group study of the doped two-dimensional hubbard model, Phys. Rev. B **95**, 125125 (2017).

[35] M. Van Damme, G. Roose, M. Hauru, and J. Haegeman, Mpskit.jl (2020).

[36] U. Schollwöck, The density-matrix renormalization group, Rev. Mod. Phys. **77**, 259 (2005).

[37] I. P. McCulloch, From density-matrix renormalization group to matrix product states, Journal of Statistical Mechanics: Theory and Experiment , 10014 (2007).

[38] N. Chepiga and F. Mila, Excitation spectrum and density matrix renormalization group iterations, Phys. Rev. B **96**, 054425 (2017).

[39] L. Vanderstraeten, F. Verstraete, and J. Haegeman, Scattering particles in quantum spin chains, Phys. Rev. B **92**, 125136 (2015).

[40] S. R. White and D. A. Huse, Numerical renormalization-group study of low-lying eigenstates of the antiferromagnetic s=1 heisenberg chain, Phys. Rev. B **48**, 3844 (1993).

[41] E. S. Sørensen and I. Affleck, Large-scale numerical evidence for bose condensation in the s=1 antiferromagnetic chain in a strong field, Phys. Rev. Lett. **71**, 1633 (1993).

[42] J. Haegeman and F. Verstraete, Diagonalizing transfer matrices and matrix product operators: A medley of exact and computational methods, Annual Review of Condensed Matter Physics **8**, 355 (2017).

[43] V. Zauner-Stauber, L. Vanderstraeten, M. T. Fishman, F. Verstraete, and J. Haegeman, Variational optimization algorithms for uniform matrix product states, Phys. Rev. B **97**, 045145 (2018).

[44] H. W. J. Blöte and Y. Deng, Cluster monte carlo simulation of the transverse ising model, Phys. Rev. E **66**, 066110 (2002).

[45] N. Bultinck, D. J. Williamson, J. Haegeman, and F. Verstraete, Fermionic matrix product states and one-dimensional topological phases, Phys. Rev. B **95**, 075108 (2017).

[46] C. S. Chiu, G. Ji, A. Bohrdt, M. Xu, M. Knap, E. Demler, F. Grusdt, M. Greiner, and D. Greif, String patterns in the doped hubbard model, Science **365**, 251 (2019).

[47] A. Bohrdt, C. S. Chiu, G. Ji, M. Xu, D. Greif, M. Greiner, E. Demler, F. Grusdt, and M. Knap, Classifying snapshots of the doped Hubbard model with machine learning, Nature Physics **15**, 921 (2019).

[48] P. Béran, D. Poilblanc, and R. Laughlin, Evidence for composite nature of quasiparticles in the 2d t-j model, Nuclear Physics B **473**, 707 (1996).

[49] R. B. Laughlin, Evidence for quasiparticle decay in photoemission from underdoped cuprates, Phys. Rev. Lett. **79**, 1726 (1997).

[50] A. Bohrdt, E. Demler, F. Pollmann, M. Knap, and F. Grusdt, Parton theory of angle-resolved photoemission spectroscopy spectra in antiferromagnetic mott insulators, Phys. Rev. B **102**, 035139 (2020).

[51] D. Poilblanc, N. Schuch, and I. Affleck, $SU(2)_1$ chiral edge modes of a critical spin liquid, Phys. Rev. B **93**, 174414 (2016).

[52] L. Vanderstraeten, E. Wybo, N. Chepiga, F. Verstraete, and F. Mila, Spinon confinement and deconfinement in spin-1 chains, Phys. Rev. B **101**, 115138 (2020).

[53] L. Vanderstraeten, M. Mariën, F. Verstraete, and J. Haegeman, Excitations and the tangent space of projected entangled-pair states, Phys. Rev. B **92**, 201111 (2015).

[54] L. Vanderstraeten, J. Haegeman, and F. Verstraete, Simulating excitation spectra with projected entangled-pair states, Phys. Rev. B **99**, 165121 (2019).

[55] B. Ponsioen and P. Corboz, Excitations with projected entangled pair states using the corner transfer matrix method, Phys. Rev. B **101**, 195109 (2020).

Appendix A: Pseudocode for excitation ansatz with open-boundary MPS

In this subsection we elaborate on the implementation details of the quasiparticle ansatz for finite systems. A finite MPS can be gauged in such a way that every tensor left and right from a given site is respectively left/right isometric

$$|\Psi(A_1 \dots A_N)\rangle = \boxed{A_1^l}\!-\!\boxed{A_2^l}\!-\!\boxed{\cdots}\!-\!\boxed{A_i^c}\!-\!\boxed{\cdots}\!-\!\boxed{A_N^r}. \quad \text{(A1)}$$

In what follows we will work in the MPO-representation of the Hamiltonian [1, 37]. We will need the partially contracted environments of the state, much like in existing DMRG codes:

$$\quad \text{(A2)}$$

We will also require V_i, the null space of A_i^l, such that

$$= 0. \quad \text{(A3)}$$

All degrees of freedom can then be absorbed in tensors X_i, as we have seen earlier

$$\boxed{B_i} = \boxed{V_i}\!-\!\boxed{X_i},$$

$$|\Phi_i(X_i)\rangle = \boxed{A_1^l}\!-\!\boxed{\cdots}\!-\!\boxed{V_i}\!-\!\boxed{X_i}\!-\!\boxed{\cdots}\!-\!\boxed{A_N^r}. \quad \text{(A4)}$$

The last two quantities we need to define are $\rho_n^{B,l}$ and $\rho_n^{B,r}$, satisfying:

$$\quad \text{(A5)}$$

and

$$\quad \text{(A6)}$$

All these quantities together make $H_{eff}(X)$ take on a pleasant form. For every site i, one has to calculate the following tensor contractions to get the derivative with respect to the tensor B_i':

$$\quad (A7)$$

The fundamental degrees of freedom are the X_i' tensors, which can then be extracted by projecting down on V_i:

$$X_i' = \quad . \qquad (A8)$$

The pseudocode for $H_{\text{eff}}(\vec{X})$ can be found in Algorithm 1. Eigenvectors can be found using any iterative eigensolver. This algorithm is very simple, straightforward to implement and requires similar contractions as in 'usual' DMRG codes. Not much changes when going to the thermodynamic limit, except the calculation for $\rho_n^{B,l}$, $\rho_n^{B,r}$ involves infinite sums [12].

Algorithm 1 Pseudocode for the action of $H_{\text{eff}}(\vec{X})$

1: Inputs $(\vec{X}, \vec{\rho^l}, \vec{\rho^r})$
2: $\vec{X}' \leftarrow 0$, $\rho^{\vec{B},l} \leftarrow 0$, $\rho^{\vec{B},r} \leftarrow 0$ ▷ initialization
3: **for** $i \in [1, len(\vec{X})]$ **do**   ▷ environments
4:      calculate $\rho_{i+1}^{B,l}$ (A5)
5:      calculate $\rho_{end-i}^{B,r}$ (A6)
6: **for** $i \in [1, len(\vec{X})]$ **do**
7:      calculate T (A7)
8:      calculate X_i' (A8)
9: **return** $\vec{X}'$